Direct Monte Carlo Simulations of Hypersonic Viscous Interactions Including Separation

James N. Moss, Didier F. G. Rault, and Joseph M. Price
NASA Langley Research Center, Hampton, Virginia 23681

Reprinted from *Rarefied Gas Dynamics: Space Science and Engineering,* edited by Bernie D. Shizgal and David P. Weaver, Vol. 160 of *Progress in Astronautics and Aeronautics,* AIAA, Washington, DC, ISBN 1-56347-081-0.

Direct Monte Carlo Simulations of Hypersonic Viscous Interactions Including Separation

James N. Moss,* Didier F. G. Rault,* and Joseph M. Price†
NASA Langley Research Center, Hampton, Virginia 23681

Abstract

Results of calculations obtained using the direct simulation Monte Carlo method for Mach 25 flow over a control surface are presented. The numerical simulations are for a 35-deg compression ramp at a low-density wind-tunnel test condition. Calculations obtained using both two- and three-dimensional solutions are reviewed, and a qualitative comparison is made with the oil flow pictures highlight separation and three-dimensional flow structure.

Introduction

Hypersonic vehicles operate over a wide range of altitude and Mach number conditions. At higher altitudes the flow is laminar and far more sensitive to separation than turbulent flows. Yet, as the flow becomes more rarefied, the highly viscous flow becomes more resistant to separation[1]; that is, the flap deflection angle required to produce separation increases with increasing rarefaction.

A motivation for studies of control surface effectiveness in rarefied flows is the desire to achieve efficient trim control of space vehicles during entry. At high altitudes, both control surfaces and control thrusters are required. Consequently, the potential exists for enhancing vehicle performance provided the control effectiveness of aerodynamic surfaces are better understood.

*Research Engineer, Space Systems Division.
†Mathematician, Space Systems Division.

Reference 2 reports on a study initiated to investigate the practicability and accuracy of the direct simulation Monte Carlo (DSMC) method to simulate viscous interacting flows resulting from flap deflections. Results of calculations for both flat plates and compression ramps compare very favorably with experimental data. The current study is a continuation of this investigation. For both studies, computations are made for test conditions reported by Chun[3-5] using two low-density wind tunnels (VG1 and VG2) at the Deutsche Forschungsanstalt fur Luft-und Raumfahrt e. V. (DLR) in Göttingen. The current study focuses on one experimental test condition where separation was observed and for the longer ramp test results reported in Ref. 5. The present two-dimensional calculations using Bird's[6] G2 code provide information on flow structure and surface quantities and how they are altered by the presence of a 35-deg ramp. In addition, the sensitivity of the calculated results to grid resolution is explored. A new feature of the present study is the use of a three-dimensional DSMC code (F3 as described in Refs. 7 and 8) to examine the effect of spanwise flow since the experiments of Chun used a finite width model where such effects are clearly evident.

Discussion

The conditions used in the numerical simulations are as follows: density $\rho_\infty = 1.401 \times 10^{-4}$ kg/m^3, velocity $V_\infty = 1.521$ km/s, and temperature $T_\infty = 9.06$ K. The freestream gas was nitrogen at a Mach number M_∞ of 24.8 and the wall temperature was specified at a constant value of 403.2 K. Furthermore, the wall was assumed to be diffuse with full thermal accommodation. The calculations allowed energy exchange between translational and internal modes. The freestream viscosity and mean free path λ_∞ were evaluated using the

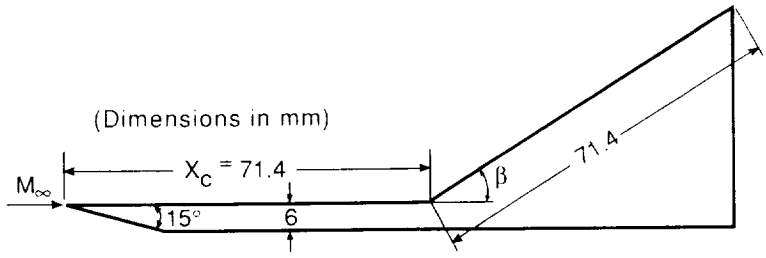

Fig. 1 Two-dimensional ramp model, 60 mm wide

variable hard sphere (VHS) collision model (see Ref. 9) with a reference temperature of 300 K and a reference diameter of 4.07×10^{-10}m. The temperature exponent of the viscosity coefficient was 0.75.

Using the above freestream specifications and the VHS collision model, the calculated freestream Reynolds number (Re_{∞,x_C}) is 12,020. The length x_C between the flat plate leading edge and the ramp corner is 71.4 mm (see Fig. 1). Also, the ramp or control flap has a length of 71.4 mm for a model wetted length of 142.8 mm. Values for Knudsen number Kn_∞ and viscous interaction parameter $\overline{V'}$ are 0.0025 and 0.14, respectively. ($\overline{V'} = M_\infty \sqrt{C'/Re_{\infty,x_C}}$ where C' is the Chapman-Rubesin viscosity constant.)

Two-Dimensional Solutions

Solutions were obtained for both a flat plate and the 35-deg ramp. For both configurations, the plate was assumed to have zero thickness. In addition, the computational domain was extended upstream of the leading edge and downstream of the trailing edge to capture upstream influence in the vicinity of the leading edge and the expansion in the near wake.

Figure 2 shows a matrix of computational and experimental conditions[3-5] in terms of ramp angle vs $\sqrt{\overline{V'}}$. Also included is an

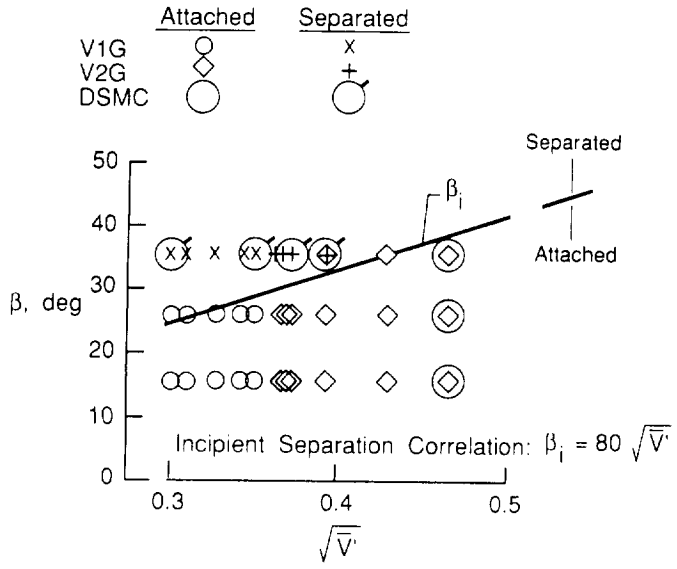

Fig. 2 Comparison of experimental and simulated results.

expression by Needham and Stollery[1] for the ramp angle to produce incipient separation. As shown, the calculations reported in Ref. 2 and the present case where $\sqrt{\overline{V'}} = 0.373$ are in agreement with the experimental data. Furthermore, the Needham-Stollery expression for incipient separation is in good agreement with the computational and experimental findings.

All of the calculated results reported in Ref. 2, with the exception of one solution ($\overline{V'} = 0.16$), were for "short" ramps where the ramp length was 31.55 mm. For these calculations and the early experimental tests[4] that used the shorter ramps, the interaction of the leading-edge shock with the ramp shock occurs near the ramp trailing edge. By doubling the ramp length, stronger shock-shock interactions occur over the ramp. Chun[5] reports that the ramp length extension seems to have no obvious influence on incipient separation. However, the topology of the reattachment is different and this may be due to the different nature of the three-dimensional interactions resulting from the two ramp lengths. Yet, the two-dimensional calculations[2] show that the ramp extension produces a somewhat larger separated region with minor changes in surface quantities.

One aspect of the present study investigated the effect of the computational grid (cell size) on computed results. The investigation was made for both a flat plate and the 35-deg compression ramp. The plate length was the same as the wetted length for the ramp, 142.8 mm. Table 1 presents a summary of the effect of cell resolution in the x and y directions as it influences the overall heat transfer

Table 1 Effect of cell resolution on flat plate solutions

Number of Cells	$\overline{C}_H$	C_D
50 x 50	0 .0074	0.0247
50 x 100	0 .0068	0.0231
50 x 150	0 .0066	0.0227
100 x 100	0 .0067	0.0229
100 x 100[a]	0 .0066	0.0226

[a]The computational domain is smaller in the y direction than that used for the other four solutions.

coefficient ($\bar{C}_H = 2Q/\rho_\infty V_\infty^3 A$ where Q is the total heat transfer rate and A the surface area) and drag coefficient ($C_D = 2D/\rho_\infty V_\infty^2 A$). Results for five combinations of cell mesh are listed. The number of cells in the x and y directions are those in the computational domain above the plate. Note that these solutions were made with three regions: one preceding the plate, one above the plate, and one following the plate. The size of the region above the plate was constant for the first four cases listed in Table 1. For the fifth case, the outer computational boundary in the y direction was moved closer to the plate surface providing a more efficient utilization of resources. The data show a much stronger dependence on the cell size in the y direction with overall heat transfer and drag coefficients decreasing with improved resolution. The flowfield and surface results presented for the plate were obtained for the fifth case listed in Table 1, where the cell dimension in the y direction in the first row of cells along the plate was less than 0.35 of the local mean free path.

For the compression ramp, the solution sensitivity to grid resolution is expressed in terms of the extent of the separation region. Table 2 lists the data for four solutions where the total number of computational cells were varied by more than an order of magnitude. These data highlight the ludicrous results that can be obtained if proper attention is not given to setting up the problem. The extent of the separation region increases by an order of magnitude as the number of cells is increased from a very coarse grid to one that approaches a grid-independent solution. All of the data presented for the ramp are from the 23,720 cell solution.

The computational domain for this solution was subdivided into seven regions to enhance flowfield resolution and to provide a more efficient use of computational resources. The region preceding the model plus the four regions above the model had the same

Table 2 Effect of cell resolution on ramp solutions

Number of Cells	Separation location, mm		Δx, mm
	x_{onset}	x_{end}	
1,950	70.0	74.3	4.3
3,675	68.8	76.3	7.5
17,725	55.8	94.7	38.9
23,720	54.7	95.7	41.0

Table 3 Effect of solution time on separation extent

Solution/Sampling time, ms		Separation location, mm		Δx,
t_{start}	t_{end}	x_{onset}	x_{end}	mm
0.45	0.80	57.8	94.1	36.3
0.87	1.27	53.9	94.7	40.8
1.27	2.49	55.5	95.2	39.7
2.49	3.85	54.7	95.7	41.0
2.49	6.09	54.7	95.7	41.0

computational time step of 1.5 x 10^{-7}s. The flow time required to achieve steady state was somewhat greater than 1 ms (Table 3). The dependence of the separation region extent on flow time is given in Table 3, demonstrating that the present results (time averaged from 2.5 to 6.1 ms) have reached steady state. The number of simulated molecules at steady state were just over 500,000, and the solution was obtained on a Sun SPARCstation 2 requiring 5.5 Mwords of memory.

Figures 3-6 present selected results of the two-dimensional simulations for both geometries. Figure 3 presents computed flowfield density contours. For the first 40 mm, the flow structure is essentially identical for both cases. In the leading-edge region, the shock wave comprises most of the shock layer, and large discrepancies exist between the calculated and Rankine-Hugoniot values of shock density. Moving farther down the flat plate, the shock density increases to a maximum value of 4.36 times the freestream value, whereas the density adjacent to the surface continues to decrease, having a value of 0.2 at the trailing edge. With the compression ramp, the influence of the ramp on the density field is evident upstream of the hinge line about 29 mm (an x value of about 42 mm). The extent of the calculated separation region can be seen in Fig. 4 where the streamlines are plotted.

Surface values for pressure coefficient ($C_p = 2\,p_w/\rho_\infty V_\infty^2$), skin-friction coefficient ($C_f = 2\tau/\rho_\infty V_\infty^2$), and heat-transfer coefficient ($C_H = 2\,q\,/\,\rho_\infty V_\infty^3$) are presented in Fig. 5 for both the geometries. These data show that the current ramp length is sufficient to capture the effects of the shock-shock interactions with the skin friction and surface pressure experiencing maximum values before reaching the ramp trailing edge. The peak heating rate and pressure values on the ramp are 15 and 32 times their respective flat plate values (for

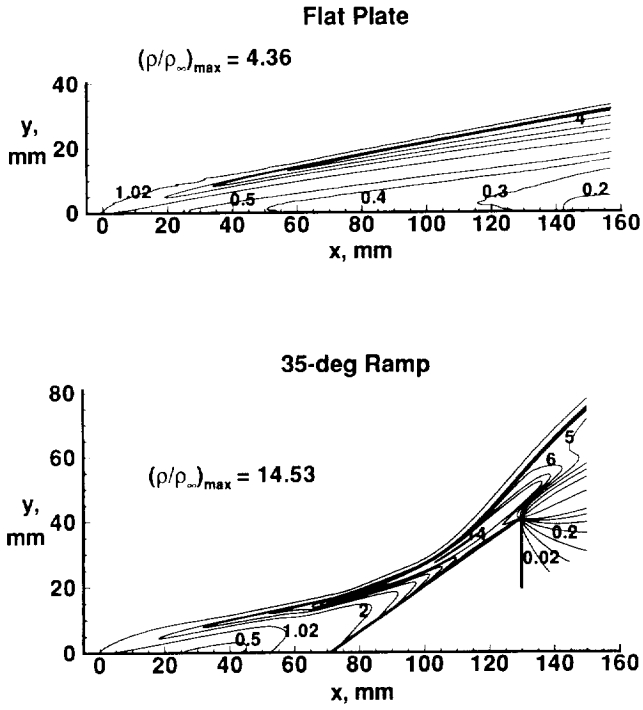

Fig. 3 Calculated density field, G2 results .

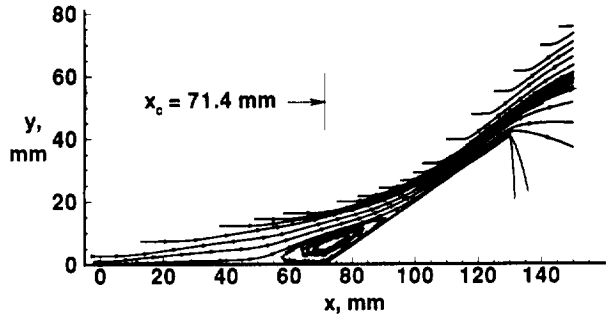

Fig. 4 Calculated streamlines, G2 results.

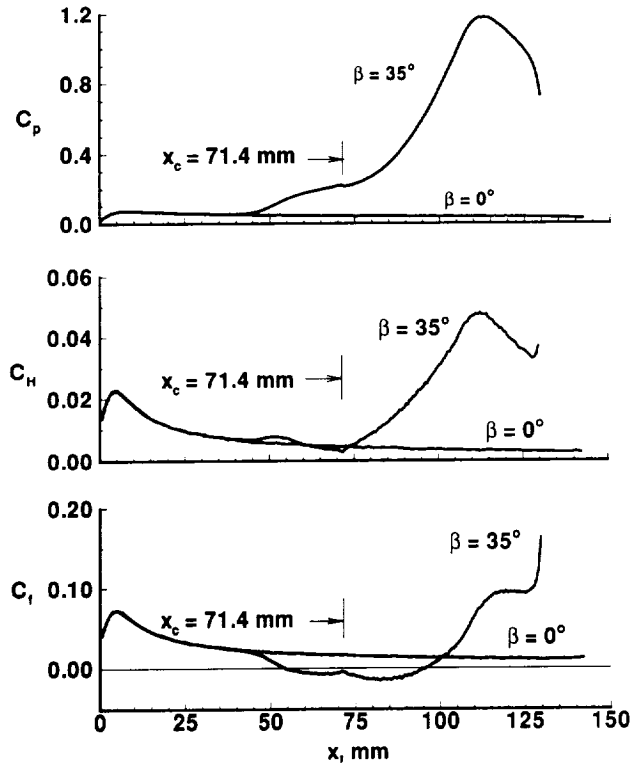

Fig. 5 Calculated pressure, heat-transfer, and skin friction coefficients, G2 results.

the same x location). Also, the effect of the trailing edge on surface quantities are clearly evident and show the expected trends; increasing heating and friction with decreasing pressure as the trailing edge is approached. The two-dimensional results presented here and in Ref. 2 show that the DSMC method, when implemented with reasonable attention to the numerical parameters (cell size, time step, time to achieve a steady state, etc.), can produce results in good agreement with experimental findings where viscous displacement, shock-shock interactions, and flow separation are significant features of the flow.

Three-Dimensional Solutions

Since experimental data from two-dimensional models have three-dimensional effects (Chun's data,[3-5] for example, where the model width was 60 mm), the ultimate test is to do numerical

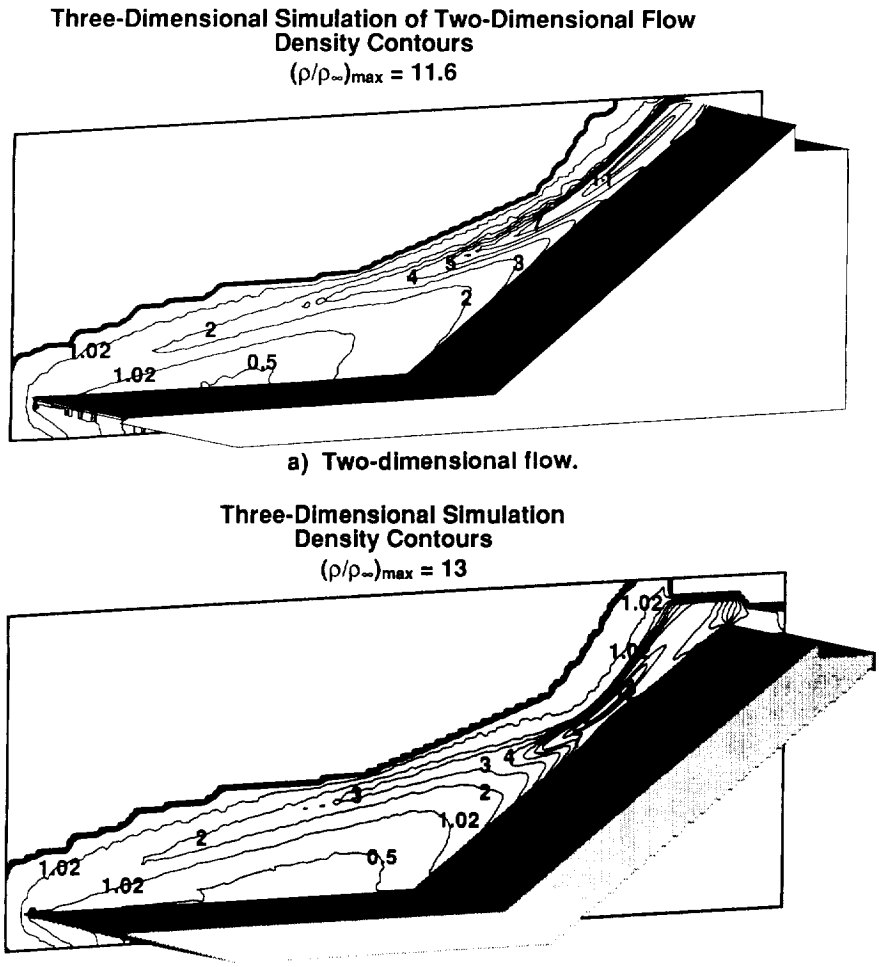

Fig. 6 Density contours resulting from three-dimensional simulations, F3 results.

simulations with a three-dimensional code. The results of Ref. 10 showed that the three-dimensional Navier-Stokes calculation provided better agreement with the experimental data than the two-dimensional calculation and that the spanwise flow was sufficient to significantly influence the flow in the center of a 61-cm wide compression corner model. A notable difference between the three-dimensional results and the two-dimensional results was a significant reduction in the size of the separated-flow region, particularly upstream of the ramp corner for the three-dimensional results.

The present three-dimensional simulations for the compression ramp are at a much more rarefied condition than those of Ref. 10, and the three-dimensional DSMC code (F3) described in Refs. 7 and 8 is used to provide the numerical simulation. The flow conditions and gas model are identical to those used in the two-dimensional simulations. The three-dimensional computations have also been made on a Sun SPARCstation 2 with 16 Mwords of memory.

The approach used for obtaining three-dimensional solutions was to first use the F3 code to simulate two-dimensional flow about the ramp and make direct comparison with the G2 results. This is accomplished by imposing a symmetry boundary condition along the outer edge of the ramp in the streamwise direction. Consequently, the computational domain is 30 mm in the spanwise direction. (The significance of the spanwise dimension is that the cell grid resolution used for this problem is similar to that used for the three-dimensional flow simulation about the ramp.) The computation included the beveled leading edge whereas the G2 solutions used a zero thickness plate followed by a wedge.

The separated region evident in the G2 calculation is also evident for the F3 results (not shown). Shown in Fig. 6a are the computed density profiles in the centerplane. The results are in general agreement with the G2 results shown in Fig. 3. Exceptions are at the leading edge of the plate and the location and magnitude of maximum density. For example, the $\rho/\rho_\infty = 1.02$ contour is located forward of the beveled leading edge, and most of the differences in the location of this contour are probably due to the beveled leading edge. However, the F3 code uses a two-level rectangular grid to define the flowfield with the finer grid used to define the surface. Consequently, any sharp leading edge will have a finite bluntness. For the present computation, the fine rectangular grid was a 0.237-mm cube (thickness of grid ratioed to the plate thickness = 0.04 or, in terms of freestream, mean free paths = $1.3\ \lambda_\infty$). This numerically induced bluntness is probably sufficient to increase the leading-edge shock angle and move the shock-shock interaction farther downstream on the ramp. This trend is clearly evident when one compares the ramp results presented in Figs. 3 and 6. Experimental evidence[11] supports this behavior and also shows that the separation length can be significantly reduced as bluntness is increased.

The computational gridding for this solution used the following arrangement: fine Cartesian grid = 612 x 219 x 126, coarse Cartesian grid = 204 x 73 x 42, unstructured cells = 28,000, and the number of simulated molecules = 500,000. For the F3 simulation of the three-dimensional flow about the ramp, the Cartesian grid was the same in the x and y directions but with a 61.9% increase in the number of grid points in the z direction. The z dimension of the computational

domain was increased from 30 to 50 mm to capture the three-dimensional effects. The number of unstructured computational cells used were 43,093 with 580,000 molecules. For both F3 simulations, a solution adaption procedure[8] was used to promote efficient use of computer resources within a memory constraint of 16 megawords. The grid restructuring was excuted several times as the solution evolved to generate cells near the body on the order of the local mean free path length in the direction normal to the body. Consequently, the unstructured cells (made up of a collection of either fine or coarse rectangular parallelepipeds) have, in general, small dimensions in the y direction and large dimensions in the x and z directions.

With the F3 code providing results for a two-dimensional problem similar to that of the G2 code, the F3 code was then used to simulate the three-dimensional flow about the compression ramp. Figure 6b shows the calculated density contours in the centerplane. The calculated three-dimensional effects are significant since the density upstream of the ramp corner is much lower than for the two-dimensional problem Fig. 6a. Also, the density in the shock-shock interaction region is noticeably higher and the shock layer thinner than that for the results shown in Fig. 6a. In addition, the streamlines (not shown) for this solution show no evidence of a vortex. When the surface shear is examined (see Ref. 9), many of the features observed in the oil-flow data (Fig. 8e of Ref. 5) such as the outflow along the side edge of the model and a very strong outflow on the wedge near the compression corner, are evident in the calculated data.

Concluding Remarks

The two- and three-dimensional DSMC computations show good qualitative agreement with existing experimental flow visulization measurements. The sensitivity of the two-dimensional solutions to grid resolution is demonstrated. The F3 compression ramp results are encouraging. First, they are in reasonably good agreement with the G2 results when the boundary conditions are modified to produce two-dimensional flows. Observed differences are possibly due to bluntness (beveled leading edge and numerical) effects at the leading edge. Subsequent numerical studies examining the effect of bluntness would be enlighting. When the F3 code simulates the three-dimensional flow about the ramp, the observed spanwise effects on flowfield and surface quantities are very significant. Additional work to extract data from the existing three-dimensional solutions will be instructive, along with additional solutions to ensure that the results are grid independent.

References

[1]Needham, D. A. and Stollery, J. L., "Boundary Layer Separation in Hypersonic Flow," AIAA Paper 66-455, June 1966.

[2]Moss, J. N., Chun, Ch.-H., and Price, J. M., "Hypersonic Rarefied Flow about a Compression Corner--DSMC Simulation and Experiment," AIAA Paper 91-1313, June 1991.

[3]Chun, Ch.-H, "Experiments on Separation at a Compression Corner in Rarefied Hypersonic Flow," Rarefied Gas Dynamics, Proceedings of the 17th International Symposium on Rarefied Gas Dynamics, edited by A. E. Beylich, VCH, Weinheim, Germany, 1991, pp. 562-569.

[4]Chun, Ch.-H, "Experimental Study of Transition Between Continuum and Molecular Flow," DFVLR-IB 222-89 A 11, March 1989.

[5]Chun, Ch.-H., "Effects of a 2-D Ramp Length Extension in Rarefied Hypersonic Flow," DLR-IB 222-91 C 18, May 1991.

[6]Bird, G. A., "The G2/A3 Program System Users Manual," Version 1.7, March 1991.

[7]Bird, G. A., "Application of the Direct Simulation Monte Carlo Method to the Full Shuttle Geometry," AIAA 90-1962, June 1990.

[8]Rault, F. G. R., "Towards an Efficient Three-Dimensional DSMC Code for Complex Geometry Problems," 18th Rarefied Gas Dynamics Symposium, Vancouver, Canada, July 1992.

[9]Bird, G. A., "Monte-Carlo Simulation in an Engineering Context, Rarefied Gas Dynamics, Progress in Astronautics and Aeronautics Vol. 74, Part I, edited by Sam S. Fisher, AIAA, New York, 1981, pp. 239-255.

[10]Rudy, D. H., Thomas, J. L., Kumar, A., Gnoffo, P. A., and Chakravarthy, S. R., "A Validation Study of Four Navier-Stokes Codes for High-Speed Flows." AIAA Paper 89-1838, June 1989.

[11]Stollery, J. L., Kumar, D., and Atcliffe, P. A., "Control Effectiveness at Hypersonic Speeds." Theroretical and Experimental Methods in Hypersonic Flows, AGARD-CP-514, April 1993, pp. 5-1 through 5-10.